Biomass Conversion and Biorefinery (2022) 12:5463–5478
https://doi.org/10.1007/s13399-020-01038-9

ORIGINAL ARTICLE

Enhanced adsorption of ciprofloxacin from aqueous solutions using functionalized banana stalk

Oluwatobi Samuel Agboola [1] · Olugbenga Solomon Bello [1,2]

Received: 12 June 2020 / Revised: 21 September 2020 / Accepted: 25 September 2020 / Published online: 9 October 2020

Abstract

Activated carbon from banana stalk, an eco-friendly agricultural waste, was prepared and investigated for its absorptive potentials in removing ciprofloxacin (CIP), an antibiotic from aqueous media. Orthophosphoric acid was used to modify the agricultural waste. The textural characteristics and adsorptive properties of the activated banana stalk (BSAC) were investigated using SEM, FTIR, Boehm titration (BT), and pH_{pzc} analytical techniques respectively. Image from the SEM of BSAC showed well-developed pores, supporting the trapping of CIP molecules to the surface, while the FTIR revealed notable bands associated with specific functional groups responsible for enhanced and efficient uptake of CIP. The Boehm titration revealed the total acidic group to be 0.699 mmol/g and the basic group to be 0.1582 mmol/g, suggesting the predominance of acidic groups, and this was supported by the pH_{pzc} value of 4.5. The most favorable interaction between the BSAC surface and the CIP molecules were in the in zwitterionic form of the CIP. The adsorptive uptake in this study was optimum at pH 8. Experimental data were studied using five different models of adsorption isotherm, namely, the Langmuir, Freundlich, Temkin, D-R, and Sips. The Langmuir isotherm ($R^2 = 0.9824$) best described the experimental data with an optimum monolayer capacity for adsorption of 49.7 mg/g at 323 K. The D-R isotherm showed that the mean free energy ranged from 1.29 to 3.54 kJ/mol, suggesting that the mechanism of adsorption for the uptake was physisorption in nature. The adsorption process was best explained by the pseudo-second-order kinetic model with R^2 values between 0.9103 and 0.9995. Thermodynamic results obtained proved that the sorption of CIP antibiotics onto BSAC was endothermic, spontaneous, and thermodynamically favored ($\Delta H = +106.561$ kJ/mol, $\Delta S = +0.44797$ kJ/mol, and $\Delta G = -36.265$ kJ/mol). BSAC prepared in this study is about six times cheaper than the commercially available activated carbon indicating the cost-effectiveness of this work. This study, therefore, establishes that the modification of banana stalk waste into activated carbon is efficient for the adsorptive uptake of ciprofloxacin antibiotics from aqueous media.

Keywords Ciprofloxacin · Banana stalk · Kinetics · Isotherm · Thermodynamics

Abbreviations

C_o	CIP initial concentration (mg l^{-1})
C_e	CIP equilibrium concentration (mg l^{-1})
C_t	CIP concentration at preset times (mg l^{-1})
V	CIP solution volume (l)
W	Mass of BSAC (g)
$q_{e(exp)}$	Amount of CIP removed by BSAC (mg g^{-1})
$q_{e(cal)}$	Calculated amount of CIP removed by BSAC (mg g^{-1})
k_{diff}	Constant of the intraparticle diffusion (mg/g $h^{1/2}$)
R_L	Separation factor of the Langmuir Isotherm
Q_m	Maximum monolayer adsorption capacity (mg g^{-1})
n	Adsorption affinity constant of the Freundlich model
B_T	Adsorption heat of the Temkin model
ΔG^o	Free energy change (J mol^{-1})
ΔH^o	Enthalpy change (J mol^{-1})
ΔS^o	Change in entropy (J mol^{-1} K^{-1})

✉ Olugbenga Solomon Bello
osbello06@gmail.com

[1] Department of Pure and Applied Chemistry, Ladoke Akintola University of Technology, P.M.B. 4000, Ogbomoso, Oyo State, Nigeria

[2] Department of Physical Sciences, Industrial Chemistry Programme, Landmark University, Omu-Aran, Nigeria

1 Introduction

The presence of antibiotics in ground and surface water has become ubiquitous in recent times. These groups of pollutants

generally referred to as "emerging pollutants" have been widely reported in aqueous environments. Antibiotics which are largely used in veterinary and human medicines have entered into water bodies through various anthropogenic activities. Unfortunately, receiving water bodies have been reported to contain these antibiotics in their metabolized and unmetabolized forms even at low concentrations. The ecological health suffers a setback by the persistence of these undesirable contaminants which accumulate in water bodies [1, 2]. The trending ability of bacteria to be resistant to antibiotics has become another growing threat to scientists as the presence of these pharmaceutical products is increasing rapidly in the environment [3–9].

Ciprofloxacin, a fluoroquinolone antibiotic, has been used in therapeutic applications both in veterinary and human medicine and has been reported to have concentrations reaching 31 mg l^{-1} or above in discharges from pharmaceutical production plants [10–12]. Due to its solubility in water, bacteria-inhibiting ability, and high molecular ring structural stability, ciprofloxacin is not easily removed from water systems [13, 14]. Antibiotics removal from waste sources has reportedly been achieved by various methods such as photodegradation, biodegradation, advanced oxidation, and adsorption [15, 16]. Unlike other treatment technologies, the adsorption process has proven better by its simple design, ease of operation, cost-effectiveness, and convenience in antibiotics removal from aqueous environments [17]. In this present study, the adsorption process is employed as an efficient, simple, and economical method for ciprofloxacin removal from contaminated water [18–20]. The cost associated with commercially available activated carbon utilized in adsorption has brought about the need to develop inexpensive adsorbent from agricultural waste materials usually of little or no economical values. Examples of such adsorbents that have been used for adsorption include rice and wheat husk [21], ground nutshell [22], waste biomass [23], and banana stalk [24, 25]. Recent advances in the adsorption of CIP have employed various adsorptive techniques such as the use of activated sludge laced with biochar derived from apple tree [26], surfactant-modified sepiolite [27], nanohybrid GO/O-CNTs [28], TiO_2 nanotube/graphene oxide hydrogel [29], Fe_3O_4/graphene oxide nanocomposite [30], and biogenic palladium nanoparticles [31] as sorbent materials. Other adsorbent materials that have been employed for the removal of other pollutants include starch/PVA composite films, ZnO–NR–AC, slag, porous carbon, carbon nanotubes, fullerenes, tire-derived carbons, multi-walled carbon nanotubes, ZnO/CuO nanocomposite, Hg-doped ZnO nanorods, bagasse fly ash, Fe@Au core–shell, ZnO/Ag nanocomposite, waste rubber tire, and rice husk [32–66].

Ortho-phosphoric acid (PA), H_3PO_4 is a common activating agent whose use has been extensively reported for preparing activated carbons from agricultural products [67–70]. PA promotes bond cleavage in the biopolymers and dehydration at low temperatures, followed by extensive cross-linking that binds volatile matter into the carbon products and thus increases the carbon yield. Benaddi et al. [71] showed that the mechanism of PA activation of biomass feedstock occurs through various steps: cellulose de-polymerization, biopolymer dehydration, formation of aromatic rings, and elimination of phosphate groups. This produces activated carbon with good yields and high surface areas. Activation conditions thus depend on the nature of the precursor, i.e., on the relative amounts of cellulose, hemicelluloses, lignin, and ashes. In the present study, authors prepared activated carbon (AC) from a banana stalk (BS) by activation with H_3PO_4; the optimum BS/PA weight/volume ratio allowing complete activation of BS was evidenced when 25.0 ± 0.01 g BS impregnated with 500 cm^3 of 0.3 mol/dm^3 ortho-phosphoric acid (H_3PO_4). The best yield was obtained using this weight/volume ratio. Alteration in the ratio of BS/PA did not produce good yield during pyrolysis [72]. Hence, this ratio was used for the acid activation.

Banana stalk, a lignocellulosic agricultural waste (which constitutes a pollutant in itself if not well disposed of), has been used in several studies as precursors in producing activated carbon [73, 74]. BSAC has been used as an efficient adsorbent in removing various pollutants such as dyes, and heavy metals in previously reported works, but the adsorption of emerging contaminants such as CIP using BSAC has not been explored. The use of carbon materials prepared from banana stalk for the sorption of ciprofloxacin antibiotics from aqueous solution, to the best of our knowledge, has not been reported. The novelty of this work is in the remarkable adsorption capacity demonstrated by the prepared adsorbent from banana stalk on ciprofloxacin (CIP) adsorption when compared with other biomass. Similarly, banana stalk can cause serious environmental threat if not properly managed; it can produce greenhouse gas if dumped in wet conditions. Usually, farmers threw the banana stalk waste in rivers and ponds where it degraded slowly and formed methane, and other gases, spreading foul smell thereby affecting the nearby ecosystem and the natural balance of atmospheric gases. It is abundantly available and has significant adsorption capacity against water-soluble pollutants (CIP inclusive). Therefore, the selection of banana stalk as an effective adsorbent material is a smart choice for sustainable future. This work, therefore, investigates the use of banana stalk as a cost-effective precursor material for preparing functionalized adsorbent for the uptake of ciprofloxacin antibiotic from aqueous solutions.

2 Materials and methods

2.1 Chemicals

Orthophosphoric acid (H_3PO_4), ciprofloxacin, NaOH, $NaHCO_3$, Na_2CO_3, and HCl are the analytical grade

chemicals used for this investigation and were not needing purification before use. The chemicals used were obtained from Aldrich Chemicals, Germany, except for ciprofloxacin (96%) which was obtained from Bond Chemicals, Aawe, Oyo State, Nigeria (Fig. 1). All chemicals were used as purchased.

2.2 Sample collection and pretreatment

Banana stalk agricultural waste was obtained from a local farm in Osun State, Oyan (a south-west town in Nigeria). The stalks were washed thoroughly with water, and impurities were further removed by rinsing with distilled water. To increase sample surface area, it was ground with mortar and pestle after the sample was sun-dried to constant weight. Uniform particle size was achieved by sieving with a 106-μm mesh size sieve.

2.3 BSAC preparation

The modification was done by reacting to 1000 ml of 0.3 M orthophosphoric acid with 50 g of banana stalk. The reaction was carried out on an electric hotplate until a slur was formed. After the slurry formation, it was carbonized at 250 °C for 3 h until a char was formed. The char formed was then washed to neutral pH with distilled water after which it is oven-dried to fixed weight at 105 °C to eliminate the moisture content and other adhering volatile materials [75]. An airtight container was used to store the banana stalk–activated carbon (BSAC) obtained for subsequent investigation.

2.4 Adsorbate preparation

Adsorbate solution stocks were prepared by the dissolution of 1.0 g CIP crystalline powder into 1000 ml of distilled water from which desired working solutions were prepared using serial dilution. Some physicochemical properties of CIP are reported in Table 1.

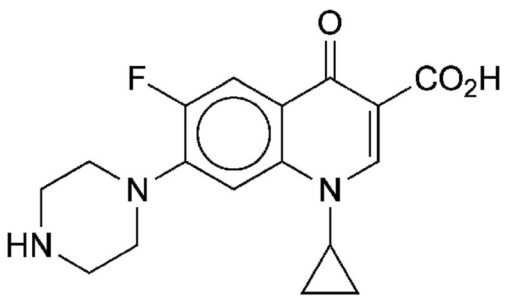

Fig. 1 Chemical structure of ciprofloxacin

2.5 BSAC characterization

2.5.1 Fourier transform infrared spectroscopy

The (FTIR) spectrometer (Perkin-Elmer FTIR-2000) was employed to record the spectra of raw banana stalk. The measurement of the spectra was obtained using a KBr disc between 4000 and 400 cm^{-1} wavelength. This analytical method was used to elucidate the characteristic functional group(s) available on the raw banana stalk sample surface.

2.5.2 Scanning electron microscopy

The morphological characteristics of the sample surface were observed with the scanning electron microscope (SEM). This electronic microscope produces enlarged images of samples [76]. Interactions of the sample's atomic constituents with the shaft of electron result into the production of different signals. Details of the sample's constituents, scenery, and the surface property were obtained from the signals generated by a scanning electron microscope [77].

2.5.3 Boehm titration

Functional groups that contain oxygen on the adsorbent surface (BSAC) were investigated using Boehm titration [78]. The workings of the Boehm titration are principled on the fact that surface oxygen groups on activated carbon have varying acidities and can be brought to neutrality using bases of different strengths [79].

2.5.4 pH point of zero charge (pH_{pzc})

The pH at which all charges on the adsorbent surface is zero is the pH_{pzc} [80]. It measures the adsorption efficiency of adsorbents in removing species from solution. The pH_{pzc} is reached when no changes occur with pH on interacting with the adsorbent(s) [81, 82].

2.6 CIP adsorption studies

2.6.1 Batch adsorption studies

The effectiveness of BSAC in removing CIP from aqueous solution was investigated at 303 K, 313 K, and 323 K using the batch adsorption method. The effect of solution temperature, contact time, and initial concentration of CIP on the adsorption process was investigated. Concentrations of 10–50 mg/l were studied. A total of 0.1 g of BSAC was carefully weighed into a 200-ml flask containing various CIP solutions (100 ml in each flask). The samples were agitated for 7 h in a water bath oscillator at a specific temperature until equilibrium was reached. Aliquots were drawn and residual

Table 1 Physicochemical properties of ciprofloxacin

Parameters	Properties
Appearance	Light yellow crystalline powder
Brand name	Ciprobay; ciproxan; cipro
Density	~ 1.5 g/cm^3
IUPAC name	1-Cyclopropyl-6-fluoro-4-oxo-7-(1-piperazinyl)-1,4-dihydro-3-quinolinecarboxylic acid
Melting point	255–257 °C
Molar mass	331.347 g/mol
Molecular formula	$C_7H_{18}FN_3O_3$
Solubility	Soluble in water

concentration measurements were taken using a spectrophotometer (UV-visible, Model 6715: JENWAY) at a preset wavelength of 273 nm. Equation (1) was used to evaluate the amount of CIP adsorbed onto BSAC.

$$q_e = \frac{(C_o - C_e)V}{W} \quad (1)$$

where the concentrations of ciprofloxacin at equilibrium and initially are C_e and C_o (mg·l^{-1}) respectively at the liquid-phase. The volume of solution and mass of BSAC used is given as V (l) and W (g) respectively.

2.6.2 Adsorption kinetics

Aliquots were drawn at specific intervals for this study and CIP measurements were taken. Eq. (2) was used to evaluate the residual concentration of CIP removed at preset times.

$$q_t = \frac{(C_o - C_e)V}{W} \quad (2)$$

where the concentrations at liquid phase of ciprofloxacin initially and at preset times are C_o and C_t (mg·l^{-1}) respectively. The volume of solution and mass of BSAC used is given as V (l) and W (g) respectively. Error bars were incorporated into different plots in this study to show the range of uncertainty or the level of accuracy of the data. The error bar also shows the range of data on the plot. The error bars in this study were evaluated for the dependent variable using the standard error obtained from the data.

3 Results and discussion

3.1 Effect of CIP initial concentration, solution temperature, and agitation time

To investigate the influence of agitation time on the adsorption process as well as the initial CIP concentration absorbed, 100 ml of initial concentrations ranging from 10 to 50 ml of the CIP solution were prepared into Erlenmeyer flasks (200 ml). An even quantity of 0.1 g of BSAC was carefully weighed into each flask, tightly closed with glass stoppers and orderly put into an isothermal water bath shaker (Model NE5.28D). The shaker was preset at 303 K and at 120 rpm rotating speed until equilibrium was attained. This process was repeated at higher temperatures (313 K and 323 K respectively) to determine the effect of solution temperature on the uptake of CIP. The amount of CIP removed increased as agitation time increased at all initial CIP concentrations. Also, as initial CIP concentration increased, the adsorbate uptake increased. The first 50 min showed rapid sorption followed by a slower sorption rate until equilibrium was reached (figure not shown).

The speedy sorption rate at the initial phase can be credited to the availability of unoccupied sites on the BSAC surface. This resulted in forces strong enough to drive the CIP molecules to overcome transfer resistance between the solid and the aqueous phase. The consequent decline in the adsorption rate must have been due to repulsion or electrostatic hindrance that exists between the adsorbent surface and CIP molecules which makes the remaining site difficult or unavailable for adsorption [83, 84]. This phase must have necessitated the adsorption process to reach equilibrium and also indicated the maximum adsorption capacity for each concentration [85].

It was observed that the different concentrations reached equilibrium at different times with the lowest initial concentration reaching equilibrium first. Experimental data shows that time to equilibrate increased with increasing initial CIP concentration. This affirms that the time to reach equilibrium for the sorption process is largely influenced by the initial antibiotic's concentration. For the removal of CIP by BSAC, the maximum adsorption removal was 9.81 mg/l at the initial CIP concentration of 10 mg/l and 45.88 mg/l at 50 mg/l initial CIP concentration. This shows also that at higher initial CIP concentration, appreciably high amount of CIP molecules was removed at equilibrium. The higher concentration gradient in the higher CIP concentrations produced a better driving force for the process [86, 87]. Cyril Dube et al. (2018) reported the

same observation for CIP removal from aqueous solutions [88].

3.2 Activation of adsorbent

The dehydration of agricultural waste materials at low temperatures through the use of orthophosphoric acid in the activation of adsorbent enhances bond cleavage in the materials [67–70]. This process of activation involves the dehydration of biopolymers, re-polymerization of cellulose with the removal of phosphate groups, and the formation of aromatic rings which yield high carbon content and good surface area activated carbon [71]. A carbon material yield generally is dependent on the nature of precursor material. Activated carbon was prepared by activating 50.0 g of BS with 1000 cm^3 of orthophosphoric acid (0.3 mol/ dm^3) in this study. This weight to volume ratio has been reported to produce the best yield [72].

3.3 Adsorbent characterization

3.3.1 Surface chemistry of BSAC

The surface properties of the prepared banana stalk were studied using FTIR. This essentially showed spectroscopic characteristics of the sample including major peaks assigned to functional groups that influence the adsorption process and suggest a possible mechanism of CIP interactions with the BSAC surface. Notable bands associated with specific functional groups that may have aided the efficient uptake of CIP were observed at 3429.55 cm^{-1} (bonded O–H group), 1616.40 cm^{-1} (carbonyl group), and 3012.91–3257.88 cm^{-1} (the secondary amine group) from the FTIR spectra of BSAC (Fig. 2). Previous studies have also reported the influence of these functional groups on adsorption processes [89–91]. Other observed bands on the BSAC which may have participated in the interactions include 1402 cm^{-1} (symmetric bending of CH_3), 1114.89 cm^{-1} (−C=O=C stretching of ether), 1242.20 cm^{-1} (–SO_3 stretching), and 648.10 cm^{-1} (–CN stretching). Ogunleye et al. (2014) reported a similar characterization result of BSAC [74]. The FTIR spectra for BSAC before and after adsorption clearly shows that the BSAC surface interacted with the CIP molecules as corresponding disappearance and appearance of new bands were observed. A slight shift in adsorption bands was also observed, all indicating the changes in spectroscopic properties of the BSAC surface having effectively adsorbed the CIP molecules. Notable changes in spectra bands after adsorption include the shift from 3429.55 to 3425.69 cm^{-1} (bonded O–H group), 3012.91–2924.18 cm^{-1} (secondary amine group).

3.3.2 pH and pH_{pzc} determinations

The pH_{pzc} of BSAC was found at 4.5 (as shown in Fig. 3). This shows that the BSAC surface is positively charged in the solution up to pH 4.5, and above this becomes negatively charged. The pH_{pzc} influenced the uptake of CIP molecules in the adsorption experiment. The pH_{pzc} of BSAC shows that cationic adsorbent uptake will be favored at pH values above the pH_{pzc} [92]. In aqueous solution, CIP molecules undergo both protonation and deprotonation reactions which give them the ability to produce three possible species of ions, which includes cationic when the pH of the solution is less than 5.9, zwitterionic when the solution pH is within the range 5.9–8.9, and anionic when solution pH is greater than 8.9 [93]. When the pH of the solution is less than 5.9, more cationic species exist which reduces CIP uptake as a result of electrostatic repulsion between the BSAC surface and the molecules of CIP. Consequently, when the value of pH is above 8.9, anions of CIP exist in solution which is favorable for the adsorption of CIP due to electrostatic exchange between the BSAC surface and CIP molecules. Nevertheless, at this pH region, there was a strong competition between the OH^- group and the CIP anionic specie for the BSAC surface which led to decreased CIP adsorption.

However, the zwitterionic species of CIP exists when the pH value is between 5.9 and 8.9 which play the most influential role in the solution as there is no repulsion or competition between the BSAC surface and the CIP molecules. Therefore, the positive BSAC surface and the zwitterionic CIP specie electrostatic interactions contributed to the high adsorption efficiency of the process. Cheng et al. (2018) and Aborode (2020) reported a similar trend on the adsorption of CIP antibiotics using halloysite nanotubes and activated kaoline respectively [94, 95]. Result from the pH studies taken in triplicates is depicted in Fig. 4 which shows that the maximum adsorption took place between pH values between 5.9 and 8.9 and at an optimum value of 8.

3.3.3 Proximate and elemental analysis

Proximate and elemental analysis was performed using a thermogravimetric analyzer (Perkin-Elmer TGA7, USA) and elemental analyzer (Perkin-Elmer series 11, 2400, USA) respectively. Proximate analysis results revealed that the percentages of moisture, fixed carbon, volatile, and ash content for BS were 14.36, 5.83, 73.91, and 5.90 respectively. On the other hand, BSAC showed low moisture and volatile content with a correspondingly high amount of fixed carbon and lower ash content with percentages of 2.91, 18.64, 73.92, and 4.53 respectively. The higher fixed carbon content value suggests that the adsorbent is favorable for the uptake of CIP antibiotics. The elemental analysis for the raw banana stalk (RBS) showed low carbon (9.32%), hydrogen (4.38%), sulfur

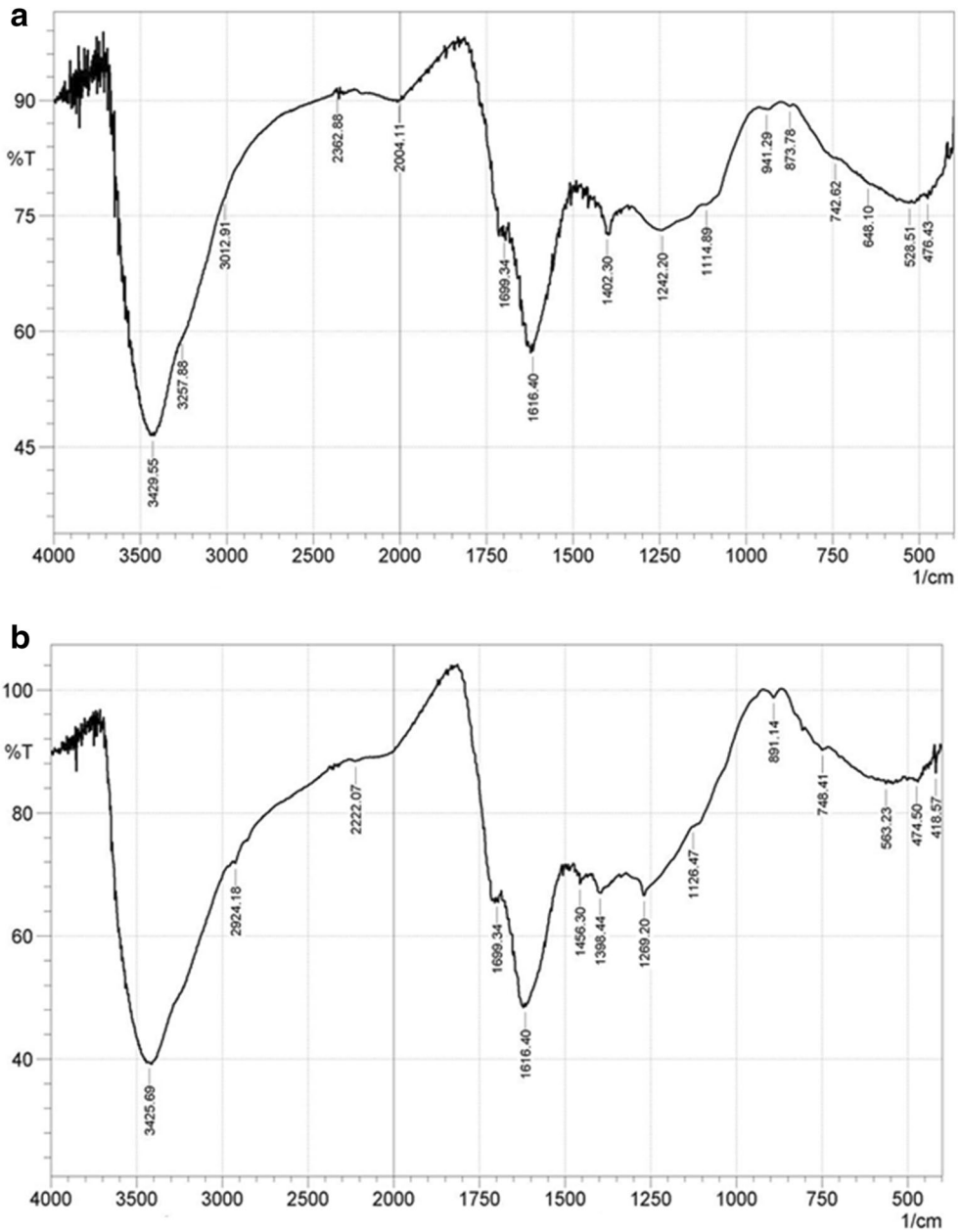

Fig. 2 **a** FTIR spectrum of acid-modified banana stalk before adsorption. **b** FTIR spectrum of acid modified banana stalk after adsorption of CIP

(0.10%) content, and high nitrogen-oxygen content combined (86.20%). The BSAC showed a very high amount of carbon (75.28), with low hydrogen (1.44%), sulfur (0.05%), and nitrogen-oxygen content combined (23.23%). This further revealed the suitability of BSAC for the uptake of CIP molecules from aqueous environments.

3.3.4 Surface morphology

Images from the SEM of BS and BSAC are respectively shown in Figs. 5a and 5b. The pores of the activated sample show that they were well-developed when compared with that of the raw sample. The improved numerous pores observed can be attributed to the influence of the acid activation in the adsorbent preparation. The better performance of BSAC in removing CIP from aqueous solution can also be attributed to the prominent and well-developed pores which allow the trapping of the CIP molecules to the surface of the BSAC.

3.3.5 Boehm's titration

Oxygen-containing functional groups usually characterize activated carbons as they influence the properties of the surfaces of carbons and their quality as adsorbents [96]. Surface acidity and basicity of adsorbents are evaluated by the Boehm's titration which assumes that NaOH, Na_2CO_3, and $NaHCO_3$ neutralize acidic groups while HCl neutralizes groups that are basic. The acid and basic groups are lactonic (0.2418 mmol/g), carboxylic

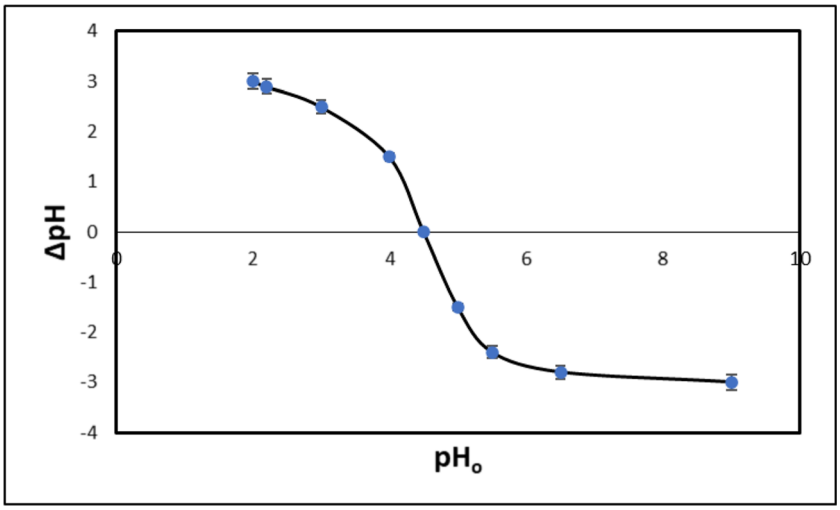

Fig. 3 Zeta potential vs. pH curve of BSAC

(0.1832 mmol/g), and phenolic (0.2749 mmol/g). The total acidic groups were 0.699 mmol/g and that of the basic groups was 0.1582 mmol/g. These results clearly show that the BSAC surface contains more acidic groups than basic groups. The surface is therefore predominantly acidic as suggested by the pH_{pzc} (4.5) value obtained [73]. This complements that cationic adsorbate will be favored in the adsorption process.

3.3.6 Adsorption kinetic studies

Four kinetic models were used in this study to investigate the kinetics of adsorption of CIP antibiotics unto BSAC. They are the pseudo-first-order (PFO), pseudo-second-order (PSO), Elovich, and the intraparticle diffusion models. Table 2 shows the adsorption kinetic data for the four models used. The PSO model described adsorption data best with a good correlation between $q_{e(exp)}$ and $q_{e(cal)}$ (Table 2), unlike the PFO model. A similar report was given by Li et al. (2018) on CIP removal using biochar obtained from used tea leaves [97]. Comparing the values of R^2 for the kinetic models used, the sorption of CIP onto BSAC was in the sequence: pseudo-second-order > pseudo-second-order > Elovich. The poor agreement of the $q_{e(exp)}$ and $q_{e(cal)}$ in the PFO model and the resulting low values of R^2 for the Elovich model makes them unsuitable to satisfactorily explain the uptake of CIP from aqueous media by adsorption.

The rate constant (k_{diff}) for the intraparticle diffusion model increased with increasing initial CIP concentration as shown in Table 2. The low R^2 values obtained showed that the model poorly fitted the adsorption data in addition to the value for the boundary layer thickness, C (mg/g), obtained in Table 2. These values showed a deviation of the linear plot from the origin. A multistep adsorption process is proposed with a gradual adsorption phase preceded by an instantaneous adsorption phase. The intraparticle diffusion is suggested to be the rate-determining step in the sorption process [98, 99]. These findings agree with studies on adsorption of CIP by rice straw biochar [100].

3.3.7 Adsorption isotherms

Studies on adsorption isotherm were investigated by fitting experimental data to five different models namely

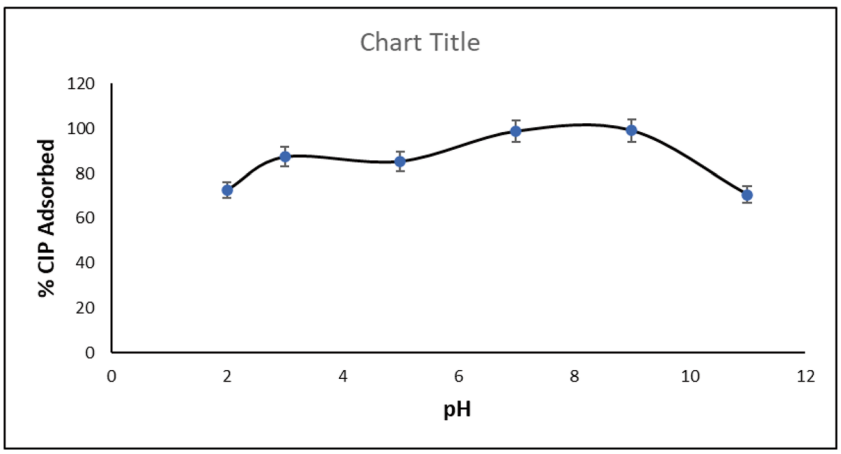

Fig. 4 Influence of pH on the adsorption of CIP by BSAC at 303 K

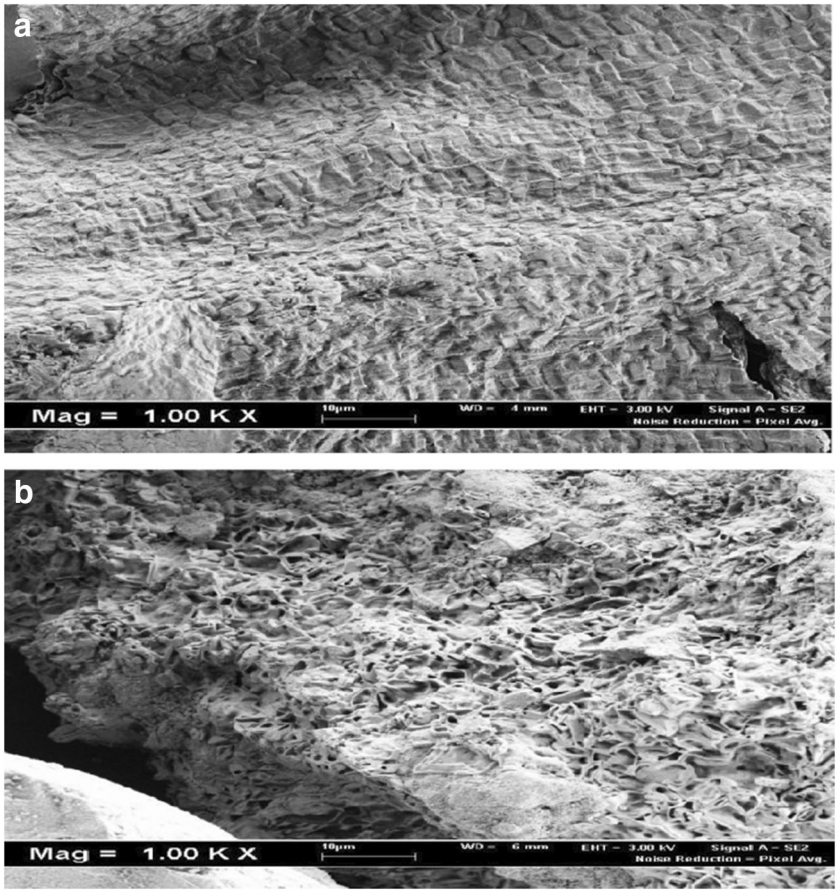

Fig. 5 SEM image of (**a**) raw BS magnification: × 1000, (**b**) BSAC magnification: × 1000

Table 2 Kinetic model parameters of CIP adsorption onto BSAC at 323 K

Model	Initial CIP concentration (mg/l)				
	10	20	30	40	50
PFO					
$q_{e(exp)}$(mg/g)	9.88177	19.6078	29.698	39.6078	45.8824
$q_{e(cal)}$(mg/g)	2.07716	6.62997	23.9723	36.3284	44.6476
k_1(min^{-1})	0.0028	0.0065	0.0085	0.0088	0.0091
R^2	0.2751	0.6947	0.9118	0.8845	0.8986
SSE (%)	0.5203	0.5643	0.1971	0.1058	1.2505
PSO					
$q_{e(exp)}$(mg/g)	9.88177	19.6078	29.698	39.6078	45.8824
$q_{e(cal)}$(mg/g)	10.0402	20.4082	32.4675	42.1941	50.0000
k_2(gmg^{-1} min^{-1})	0.02238	0.00372	0.0006	0.00039	0.0003
R^2	0.9995	0.9981	0.9548	0.9103	0.9212
SSE (%)	0.0106	0.0348	0.0955	0.0834	0.1328
Elovich					
β	0.68639	0.34214	0.21081	0.16409	0.14275
α	8.18501	9.5821	0.8907	4.11618	0.8335
R^2	0.8063	0.9484	3.59422	0.853	4.49789
Intraparticle diffusion					
C	5.5231	8.5408	5.2488	5.9193	5.8649
k_{diff}	0.301	0.7009	1.3048	1.6887	2.0000
R^2	0.4881	0.7734	0.9557	0.929	0.9634

Langmuir, Temkin, Dubinin-Radushkevich, Freundlich, (two-parameter isotherm models), and Sips isotherm (three-isotherm model) respectively. The R^2 values of the different isotherms were compared to ascertain the isotherm that best explained the adsorption process. Results from the adsorption models used in this study are presented in Table 3. Figure 6 a, b, c, and d also show various plots from isotherm models. The Langmuir isotherm assumes the surface is covered as monolayer by an adsorbate when maximum monolayer adsorption has occurred. The best adsorption capacity that correlates with monolayer coverage on the BSAC can be evaluated by this adsorption isotherm. Q_m for the Langmuir isotherm was 49.75 mg/g at 323 K with an R^2 value of 0.9824. This indicates that the experimental data fitted well into the isotherm model. The separation factor (R_L) value ranged between zero and unity which indicated the favorability of the process and the good fitting of the data to the Langmuir isotherm [101].

The value of $n > 1$ in the Freundlich model shows that the sorption process was simple, favorable, and physical [102–104]. Table 3 shows that the k_f values increased with increasing temperature which suggested a higher affinity of the BSAC for CIP molecules at higher temperatures. The constant B_T of the Temkin model which relates to adsorption heat has a positive value of 295.47 ($R^2 = 0.6669$) suggesting an endothermic process for the adsorption. The mean free energy of the D-R model was within the range of 1.29–3.54 kJ/mol which is lesser than 8 kJ/mol suggesting that the adsorption mechanism is physical [105, 106]. The Q_m of the D-R model follows closely the Langmuir Q_m and with a value of 47.89 mg/g ($R^2 = 0.8137$). The three-parameter isotherm model, Sips, gave the least Q_{max} of 43.08 mg/g with an R^2 value of 0.9043.

Judging from the R^2 values vis-à-vis their Q_{max}, the adsorption of CIP unto BSAC followed this order of fitness of isotherm model to experimental data: Langmuir (0.9824) > Sips (0.9043) > D-R (0.8137) > Temkin (0.6669) > Freundlich (0.5864). This order implies that the Langmuir isotherm best explains the experimental data. Table 4 shows the CIP adsorption capacities of different adsorbent materials. BSAC gave the highest Q_{max} value compared with other adsorbents.

Table 3 Adsorption isotherm parameters for CIP removal using BSAC

	Parameters	303 K	313 K	323 K
Langmuir	q_m (mg/g)	80.64516	30.8642	49.75124
	K_L (l/mg)	0.214905	2.892857	2.871429
	R_L	0.085141	0.006866	0.001355
	R^2	0.9692	0.9998	0.9824
Freundlich	K_f (mg/g(l/mg))$^{1/n}$	13.92515	19.1602	33.32729
	n	1.406866	4.370629	2.768549
	R^2	0.9791	0.9518	0.5864
Temkin	B_T	157.7915	575.7771	295.4682
	K_t	2.579441	110.3098	51.50082
	R^2	0.9784	0.9905	0.6669
D-R	E (kJ/mol)	1.29	4.08	3.5435
	Q_m (mg/g)	37.70905	28.7288	47.89926
	R^2	0.9233	0.9163	0.8137
	β (mol^2.kJ^{-2})	0.0003	3.00E-05	4.00E-08
Sips	Ks	0.2494	1.486	9.677
	q_m (mg/g)	70.97	37.02	43.08
	n	0.9211	1.708	0.6139
	R^2	0.9984	0.9989	0.9043

3.3.8 Adsorption thermodynamic studies

Thermodynamic parameters at three different temperatures were investigated in this study using the equations below.

$$\ln K_L = \frac{\Delta S^0}{R} - \frac{\Delta H^0}{RT} \quad (3)$$

$$\Delta G^0 = -RT \ln(55.5\, K_L) \quad (4)$$

$$E_a = \Delta H^0 + RT \quad (5)$$

Since K_L is expressed in l.mol^{-1}, then K_L can be recalculated as dimensionless by multiplying it by 55.5 (number of moles of water per liter of solution). Accordingly, the correct ΔG^0 value can be obtained from Eq. (4). Here, ΔG^0 is the standard Gibbs free energy change (kJ mol^{-1}), R is the universal gas constant (8.314 J mol^{-1} K^{-1}), T is the absolute temperature (K), and E_a (KJ/mol) is the Arrhenius energy. ΔH^0 and ΔS^0 values of the adsorption process were calculated from the Van't Hoff Equation (Eq. 4). The values of $\Delta H°$ and $\Delta S°$ values were calculated from the slope and intercept of the plot of ln (K_L) versus 1/T, they are listed in Table 5. The results from standard free energy (ΔG^0), entropy (ΔS^0), and enthalpy (ΔH^0) changes were employed to report the feasibility, spontaneity, and nature of the sorption process as given by the Eqs. (3), (4), and (5). Table 5 shows the thermodynamic values obtained. The negative ΔG^0 values suggest that the uptake of CIP by BSAC was spontaneous and thermodynamically favored. ΔG^0 values increased with an increase in temperature which suggests that the adsorption was more spontaneous at higher temperatures. Positive ΔH^0 value indicated the process is endothermic and the increased randomness at the solid-liquid interface in the course of the adsorption of CIP unto BSAC was established by the positive value of ΔS^0. Sharifpour et al. reported a similar observation for removal of CIP using activated carbon with multi-walled carbon nanotubes [103, 119].

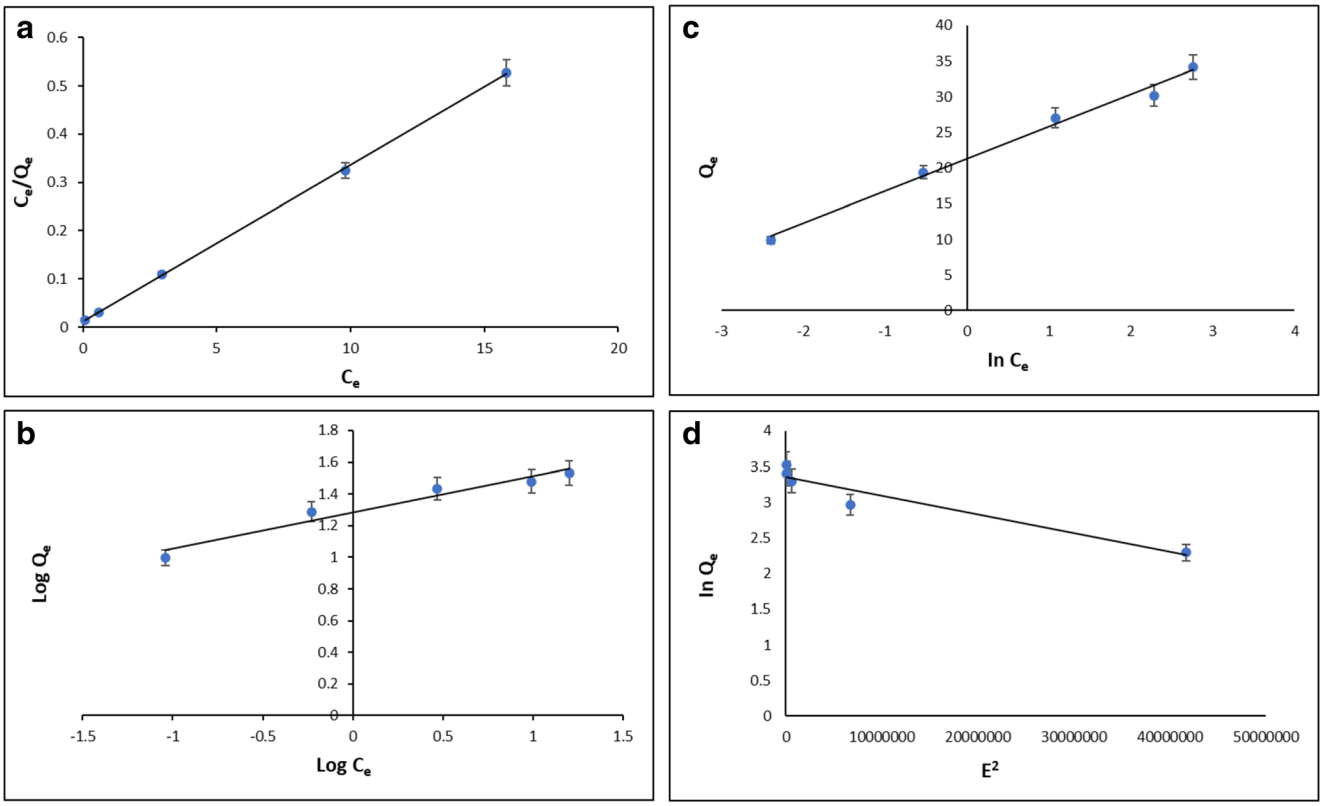

Fig. 6 Plot of Langmuir (**a**), Freundlich (**b**), Temkin (**c**), and D-R (**d**) isotherm at 313 K

Table 4 Maximum monolayer adsorption capacities of CIP adsorption on different adsorbents

Adsorbent	Q_{max} (mg/g)	pH	Temp (K)	Adsorbent dose (g)	Time (min)	Initial conc. (mg/l)	Refs.
Aluminum hydrous oxide	14.72	7.1	298	0.03	1440	–	[107]
Iron hydrous oxide	25.76	7.1	298	0.03	1440	–	120
Kaolinite	6.99	3.5	–	1.0	480		[108]
Pomegranate Peel	2.353	8	298	0.05	150	50	[109]
MgO nanoparticles	3.46	6	–	1	60	10	[110]
Red mud	19.12	7	303	5	75	50	[111]
Apple tree–derived biochar	20.7	6.3	–	0.1	1440	250	26
KOH-modified biochar	23.36	8.6	308.15	0.01	720	16	[112]
Fe_3O_4 nanoparticles	24	8	298	2.5	360	100	[113]
Nanotube structured hallo site	21.7	6	–	1.0	300	10	[114]
Potato stems and leaves	11.5	10	298	2.0	1440	10	[115]
Activated kaolin	17.9	4	298	0.2	120	120	[95]
Bamboo charcoal	36.02	5.5	298	0.1	720	25	[116]
Humic acid/cellulose nanocomposite	10.87	–	318	0.1	1440	10	[117]
Graphene oxide/calcium alginate	39.06	5.9	293	2.0	1440	60	[118]
BSAC	*49.75*	*8*	*323*	*0.1*	*420*	*50*	*This work*

Core findings of our investigation are presented in italics

Table 5 Thermodynamic parameters for the adsorption of CIP unto BSAC

Temp (K)	K_o (l/mol)	ΔG (kJ/mol)	ΔH (kJ/mol)	ΔS (kJ/mol)	E_a (kJ/mol)
303	71,208	− 36.265	106.561	0.44797	0.10908
313	958,540	− 46.293			0.109163
323	951,439	− 47.752			0.109246

3.3.9 Adsorption mechanism

Consequent to results obtained from the pH studies, a likely mechanism of adsorption was inferred. The basic functional groups on both the surface of the BSAC and the CIP molecules largely influences the mechanism of the adsorption as the pH of solution was varied between 3 and 11. Maximum adsorption was observed within pH 6.5 and 9.0. At this pH range, electrostatic interaction between BSAC surface functional groups and the CIP charged molecules occurred, i.e., between the negatively charged carbon-oxygen groups (carbonyl and hydroxyl groups) present on the BSAC surface and the positively charged amine group in the zwitterionic specie of the CIP (mechanism shown in Fig. 7 a and b). However, the slight decrease in adsorption at pH between 9.0 and 11.0 was attributed to repulsion between the negatively charged adsorbent surface and the carboxylate group on the CIP that is negatively charged. The electrostatic repulsion is suspected to have dominated the adsorption in this phase. At pH above 9.0, both the CIP and BSAC remains negatively charged in solution. This led to a resultant decrease in the uptake of CIP by the adsorbent. Summarily, a fairly good uptake is observed at pH < 4.5 and pH > 8.5. Hence, a hydrogen bonding mechanism is proposed to have taken place particularly at pH > 8.5 where the adsorbent surface containing carbonyl groups could form hydrogen bonding (and possibly a dimmer) with the carbonyl groups on the CIP molecules (mechanism shown in Fig. 7c). Therefore, hydrogen bonding and electrostatic interactions are proposed mechanisms for the adsorption of CIP onto BSAC surface. Wang et al. (2010), Punyapalakul and Sitthisom (2010), and El-shafey et al. (2012) also reported a similar mechanism in the adsorption of CIP unto montmorillonite, modified silicates, and activated carbon prepared from date palm leaflets respectively [120–122].

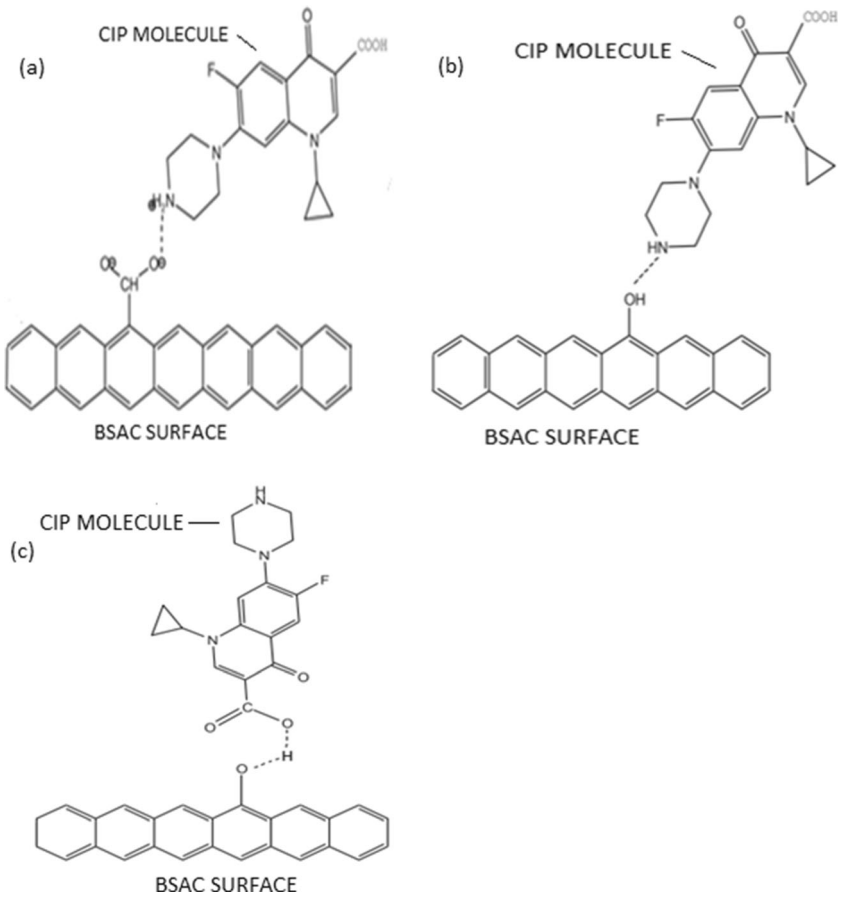

Fig. 7 Adsorption mechanism showing (**a** and **b**) electrostatic attraction between the negatively charged carbon-oxygen groups on BSAC surface and the positively charged amine group on the CIP molecule, (**c**) hydrogen bonding between carbonyl groups on BSAC surface and carbonyl groups on the CIP molecule

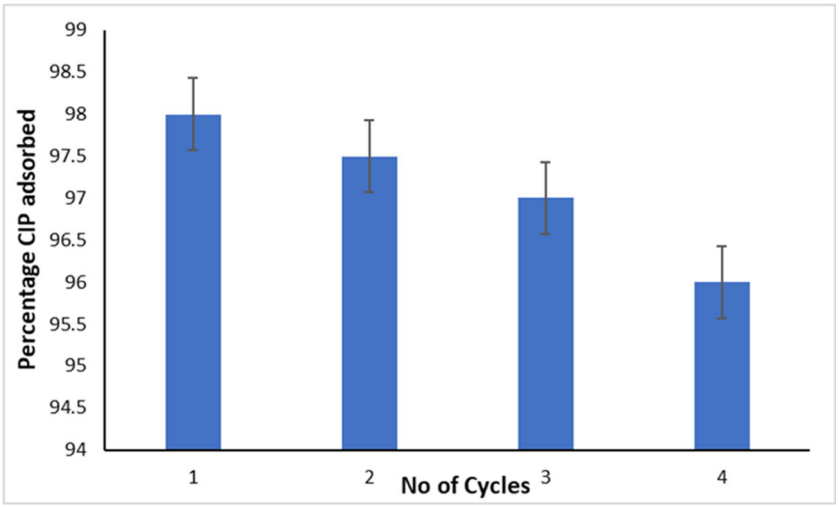

Fig. 8 The reusability of BSAC for the removal of CIP for 4 cycles (each cycle stood for 50 min)

3.3.10 Regeneration and reusability studies

Adsorbent reusability is an important parameter in determining their economic feasibility [123, 124]. For this to be accomplished, the adsorbent was regenerated first using different solvents and re-used over several cycles to check whether there is appreciable performance decline. Three different solvents were used for regeneration; they are water (H_2O), hydrochloric acid (HCl), and sodium hydroxide (NaOH). The potential of the eluents used in regeneration follows the order H_2O (95.12%) > HCl (81.62%) > NaOH (55.47%). Since water gave the highest desorption, it was used to desorb CIP molecules from BSAC over several cycles. It was observed that the percentage adsorption of CIP remained fairly constant without significant change for 4 cycles (Fig. 8). For accuracy purposes, 2% decrease in the values of percentage of CIP adsorbed was observed between the 1st and 4th cycles (Fig. 8). Apparently, the results obtained proved that the BSAC desorbed with water after each adsorption step has the ability to work with high efficiency for CIP removal from aqueous solution. The results obtained from this study proved that BSAC has attractive features (e.g., recycling, cheap, flexibility, fast adsorption kinetics, handling, and large adsorption capacity) that encourage their practical applications in wastewater management.

Table 6 Comparison of price between BSAC and CAC

Cost description	Price (USD)	
	BSAC (1 kg)	CAC (1 kg)
Distilled water	11.86	
Orthophosphoric acid	17.56	
Transportation	10.00	5.0
Electricity	4.00	
Filter paper	3.22	
Cost of purchase	–	300
Total	46.64	305
Difference (CAC-BSAC)	258.36	

3.4 Cost analysis

Table 6 shows the cost analysis of BSAC in comparison with commercial activated carbon (CAC). Activated carbon prepared in this study is approximately five and a half times cheaper than the CAC saving cost up to USD 258 per kilogram. The cost implication and the summary of all essential expenses made in the preparation of BSAC are shown in Table 6. The cost of orthophosphoric acid and distilled water accounts for the greater percentage of the total cost in the preparation.

4 Conclusion

This study shows the effectiveness of agricultural waste biomass, banana stalk, when functionalized with orthophosphoric acid in the adsorption of ciprofloxacin antibiotic from aqueous media. Well-developed pores from the SEM, high carbon content from the proximate and elemental analysis, and the observed functional groups from the FTIR demonstrated the suitability of the adsorbent in removing CIP antibiotics from aqueous solution. The Langmuir isotherm model best describes the adsorption data, thus establishing that the uptake of CIP was of a monolayer approach on the BSAC surface. Experimental data were best explained by the pseudo-second-order kinetic model and adsorption mechanism was mainly controlled by the intraparticle diffusion model. Thermodynamic studies revealed that the free energy change was negative, while the enthalpy and entropy values were positive, indicating that the sorption process is endothermic

and spontaneous. This study reveals that banana stalk, an inexpensive activated carbon precursor, can efficiently remove CIP from aqueous solutions.

Funding The corresponding author acknowledges the supports obtained from The World Academy of Science (TWAS) in the form of research grants: research grant number: 11–249 RG/CHE/AF/AC_1_UNESCO FR: 3240262674 (2012), 15–181 RG/CHE/AF/AC_1_:3240287083 (2015) for the purchase of research equipment, and LAUTECH 2016 TET Fund Institution Based Research Intervention (TETFUND/DESS/UNI/OGBOMOSO/RP/VOL. IX) respectively.

References

1. Burakov AE, Galunin EV, Burakova IV, Kucherova AE, Agarwal S, Tkachev AG, Gupta VK (2018) Adsorption of heavy metals on conventional and nanostructured materials for wastewater treatment purposes: a review. Ecotoxicol Environ Saf 148:702–712
2. Gupta VK, Saleh TA (2013) Sorption of pollutants by porous carbon, carbon nanotubes and fullerene – an overview. Environ Sci Pollut Res 20(5):2828–2843
3. Grice HC, Goldsmith LA (2000) Sucralose: an overview of the toxicity data. Food Chem Toxicol 38:1–6
4. Corbel V, Stankiewicz M, Pennetier C, Fournier D, Stojan J, Girard E, Dimitrov M, Molgó J, Hougard JM, Lapied B (2009) Evidence for inhibition of cholinesterases in insect and mammalian nervous systems by the insect repellent deet. BMC Biol 7:47
5. Ricart M, Guasch H, Alberch M, Barceló D, Bonnineau C, Geiszinger A, Farré M, Ferrer J, Ricciardi F, Romaní AM, Morin S, Proia L, Sala L, Sureda D, Sabater S (2010) Triclosan persistence through wastewater treatment plants and its potential toxic effects on river biofilms. Aquat Toxicol 100:346–353
6. Heberer T (2002) Occurrence, fate, and assessment of polycyclic musk residues in the aquatic environment of urban areas e a review. Acta Hydrochim Hydrobiol 30:227–243
7. McArthur JV, Tuckfield RC (2000) Spatial patterns in antibiotic resistance among stream bacteria: effects of industrial pollution. Appl Environ Microbiol 66:3722–3726
8. Martínez JL (2008) Antibiotics and antibiotic resistance genes in natural environments. Science 321:365–367
9. Watkinson AJ, Murby EJ, Kolpin DW et al (2009) The occurrence of antibiotics in an urban watershed: from wastewater to drinking water. Sci Total Environ 407:2711–2723
10. Mostafaloo R, Asadi-Ghalhari M, Izanloo H, Zayadi A (2020) Photocatalytic degradation of ciprofloxacin antibiotic from aqueous solution by $BiFeO_3$ nanocomposites using response surface methodology. Global Journal of Environmental Science and Management 6(2):191–202
11. Carmosini N, Lee LS (2009) Ciprofloxacin sorption by dissolved organic carbon from reference and bio-waste materials. Chemosphere 77:813–820
12. Larsson DGJ (2008) Drug production facilities – an overlooked discharge source for pharmaceuticals to the environment, in Kümmerer K. (Ed.) Pharmaceuticals in the environment: sources, fate, effects and risks, *Springer Berlin Heidelberg, Berlin, Heidelberg*, pp. 37–42
13. Genc N, Dogan EC (2015) Adsorption kinetics of the antibiotic ciprofloxacin on bentonite, activated carbon, zeolite, and pumice. Desalin Water Treat 53:785–793
14. Singla P, Goel N, Singhal S (2016) Affinity of boron nitride nanomaterials towards antibiotics established by exhaustive experimental and theoretical investigations. Chem Eng J 299:403–414
15. Balarak D, Mostafapou FK, Joghataei A (2016) Experimental and kinetic studies on penicillin G adsorption by Lemnaminor. British Journal of Pharmaceutical Research 9(5):1–10
16. Balarak D, Azarpira H (2016) Photocatalytic degradation of sulfamethoxazole in water: investigation of the effect of operational parameters. International Journal of Chem Tech Research 9(12): 731–738
17. Choi KJ, Kim SG, Kim SH (2008) Removal of antibiotics by coagulation and granular activated carbon filtration. J Hazard Mater 151:38–43
18. Pham TD, Vu TN, Nguyen HL, Le PHP, Hoang TS (2020) Adsorptive removal of antibiotic ciprofloxacin from aqueous solution using protein-modified nanosilica. Polymers 12:57
19. Zhang W, He G, Gao P, Chen G (2003) Development and characterization of composite nanofiltration membranes and their application in concentration of antibiotics. Sep Purif Technol 30:27–35
20. Balarak D, Azarpira H (2016) Rice husk as a biosorbent for antibiotic metronidazole removal: isotherm studies and model validation. International Journal of Chemical Technology Research 9(7): 566–573
21. Rao MM, Roddy DHKK, Venkateswarth P, Seshaiah P (2009) Removal of mercury from aqueous solutions using activated carbon prepared from agricultural by-product-waste. J Environ Manag 90(1):634–643
22. Isah UA, Yusuf AI (2012) Adsorption of lead ions on groundnut shell activated carbon. Der Chemica Sinica 3(6):1511–1515
23. Erdem M, Ucar S, Karagöz S. and Tay, T. (2013). Removal of lead (II) ion from aqueous solution onto activated carbon derived from waste biomass. *Scientific World Journal,* June 18.https://doi.org/10.1155/2013/146092
24. Salman JM, Hameed BH (2010) Removal of insecticide carbofuran from aqueous solutions by banana stalks activated carbon. J Hazard Mater 176:814–819
25. Hameed BH, Mahmoud DK, Ahmad AL (2008) Sorption equilibrium and kinetics of basic dye from aqueous solution using banana stalk waste. J Hazard Mater 158:499–506
26. Kim DG, Choi D, Cheon S, Ko S, Kang S, Oh S (2020) Addition of biochar into activated sludge improves removal of antibiotic ciprofloxacin. Journal of Water Process Engineering 33:101019
27. Balarak D, Zafariyan M, Siddiqui S (2020) Investigation of adsorptive properties of surfactant modified sepiolite for removal of ciprofloxacin. International Journal of Life Science and Pharma Research 10(3):12–19
28. Mohammad MF, Fahmi AA, Ahmad RM (2020) Ultimate eradication of the ciprofloxacin antibiotic from the ecosystem by nanohybrid GO/O-CNTs. ACS Omega 5:4457–4468
29. Yuan Z, Fei Y, Jie M. (2015) Enhanced adsorption and removal of ciprofloxacin on regenerable long TiO_2 nanotube/graphene oxide hydrogel adsorbents. *Journal of Nanomaterials*. https://doi.org/10.1155/2015/675862
30. Balarak D, Zafariyan M, Chandrika K (2020) Adsorption of ciprofloxacin from aqueous solution onto Fe_3O_4/graphene oxide nanocomposite. Int J Pharm Sci Res 11(1):268–274
31. He P, Mao T, Wang A, Yin Y, Shen J, Chen H, Zhang P (2020) Enhanced reductive removal of ciprofloxacin in pharmaceutical wastewater using biogenic palladium nanoparticles by bubbling H_2. Royal Society of Chemistry Advances 10:26067–26077
32. Priya B, Gupta VK, Pathania D, Singha AS (2014) Synthesis, characterization and antibacterial activity of biodegradable starch/PVA composite films reinforced with cellulosic fibre. Carbohydr Polym 109:171–179
33. Dil EA, Ghaedi M, Ghaedi AM, Asfaram A, Goudarzi A, Hajati S, Agarwal MS, Gupta VK (2016) Modeling of quaternary dyes adsorption onto ZnO–NR–AC artificial neural network: analysis by derivative spectrophotometry. J Ind Eng Chem 34:186–197

34. Gupta VK, Carrott PJM, Singh R, Chaudhary M, Kushwaha S (2015) Cellulose: a review as natural, modified and activated carbon adsorbent. Bioresour Technol 216:1066–1076
35. Nekouei F, Nekouei S, Tyagi I, Gupta VK (2015) Kinetic, thermodynamic and isotherm studies for acid blue 129 removal from liquids using copper oxide nanoparticle-modified activated carbon as a novel adsorbent. J Mol Liq 201:124–133
36. Gupta VK, Rastogi A, Dwivedi MK, Mohan D (1997) Process development for the removal of zinc and cadmium from wastewater using slag—a blast furnace waste material. Sep Sci Technol 32(17):2883–2912
37. Mittal A, Mittal J, Malviya A, Gupta VK (2010) Removal and recovery of Chrysoidine Y from aqueous solutions by waste materials. J Colloid Interface Sci 344(2):497–507
38. Gupta VK, Jain R, Nayak A, Agarwal S, Shrivastava M (2011) Removal of the hazardous dye—tartrazine by photodegradation on titanium dioxide surface. Mater Sci Eng C 31(5):1062–1067
39. Saleh TA, Gupta VK (2012) Photo-catalyzed degradation of hazardous dye methyl orange by use of a composite catalyst consisting of multi-walled carbon nanotubes and titanium dioxide. J Colloid Interface Sci 371(1):101–106
40. Gupta VK, Nayak A, Agarwal S (2015) Bioadsorbents for remediation of heavy metals: current status and their future prospects. Environmental Engineering Research 20:001–018
41. Saleh TA, Gupta VK (2014) Processing methods, characteristics and adsorption behavior of tire derived carbons: a review. Adv Colloid Interf Sci 211:92–100
42. Saravanan R, Sacari E, Gracia F, Khan MM, Mosquera E, Gupta VK (2016) Conducting PANI stimulated ZnO system for visible light photocatalytic degradation of coloured dyes. J Mol Liq 221: 1029–1033
43. Rajendran S, Khan MM, Gracia F, Qin J, Gupta VK, Arumainathan S (2016) Ce(3+)-ion-induced visible-light photocatalytic degradation and electrochemical activity of ZnO/CeO_2 nanocomposite. Sci Rep 6:31641
44. Saravanan R, Karthikeyan S, Gupta VK, Sekaran G, Narayanan V (2013) Enhanced photocatalytic activity of ZnO/CuO nanocomposite for the degradation of textile dye on visible light illumination. Mater Sci Eng C 33(2013):91–98
45. Saravanan R, Thirumal E, Gupta VK, Narayanan V, Stephen A (2013) The photocatalytic activity of ZnO prepared by simple thermal decomposition method at various temperatures. J Mol Liq 177:394–401
46. Saravanan R, Gupta VK, Prakash T, Narayanan V, Stephen A (2013) Synthesis, characterization and photocatalytic activity of novel hg doped ZnO nanorods prepared by thermal decomposition method. J Mol Liq 178:88–93
47. Saleh TA, Gupta VK (2011) Functionalization of tungsten oxide into MWCNT and its application for sunlight-induced degradation of rhodamine B. J Colloid Interface Sci 362(2):337–344
48. Saleh TA, Gupta VK (2011) Photo-catalyzed degradation of hazardous dye methyl orange by use of a composite catalyst consisting of multi-walled carbon nanotubes and titanium dioxide. J Colloid Interface Sci 371(1):101–106
49. Gupta VK, Sharma S (2003) Removal of zinc from aqueous solutions using bagasse fly ash − a low cost adsorbent. Ind Eng Chem Res 42(25):6619–6624
50. Ahmaruzzaman M, Gupta VK (2011) Rice husk and its ash as low-cost adsorbents in water and wastewater treatment. Ind Eng Chem Res 50(24):13589–13613
51. Mohammadi N, Khani H, Gupta VK, Amereh E, Agarwal S (2011) Adsorption process of methyl orange dye onto mesoporous carbon material–kinetic and thermodynamic studies. J Colloid Interface Sci 362(2):457–462
52. Saleh TA, Gupta VK (2012) Synthesis and characterization of alumina nano-particles polyamide membrane with enhanced flux rejection performance. Sep Purif Technol 89:245–251
53. Saravanan R, Khan MM, Gupta VK, Mosquera E, Gracia F, Narayanan V, Stephen A (2015) ZnO/Ag/CdO nanocomposite for visible light-induced photocatalytic degradation of industrial textile effluents. J Colloid Interface Sci 452:126–133
54. Saravanan R, Khan MM, Gupta VK, Mosquera E, Gracia F, Narayanan V, Stephen A (2015) ZnO/Ag/Mn_2O_3 nanocomposite for visible light-induced industrial textile effluent degradation, uric acid and ascorbic acid sensing and antimicrobial activity. RSC Adv 5:34645–34651
55. Ghaedi M, Hajjati S, Mahmudi Z, Tyagi I, Agarwal S, Maity A, Gupta VK (2015) Modeling of competitive ultrasonic assisted removal of the dyes – methylene blue and Safranin-O using Fe_3O_4 nanoparticles. Chem Eng J 268:28–37
56. Gupta VK, Nayak A, Agarwal S, Tyagi I (2014) Potential of activated carbon from waste rubber tire for the adsorption of phenolics: effect of pre-treatment conditions. J Colloid Interface Sci 417:420–430
57. Saravanan R, Joicy S, Gupta VK, Narayanan V (2013) Visible light induced degradation of methylene blue using CeO2/V2O5 and CeO2/CuO catalysts. Mater Sci Eng C 33:4725–4731
58. Saravanan R, Karthikeyan N, Gupta VK, Thirumal E, Thangadurai P, Narayanan V, Stephen A (2013) ZnO/Ag nanocomposite: an efficient catalyst for degradation studies of textile effluents under visible light. Mater Sci Eng C 33(4):2235–2244
59. Saravanan RM, Khan M, Gupta VK, Mosquera E, Gracia F, Narayanan V, Stephen A (2015) nO/Ag/CdO nanocomposite for visible light-induced photocatalytic degradation of industrial textile effluents. J Colloid Interface Sci 452:126–133
60. Asfaram A, Ghaedi M, Agarwal S, Tyagi I, Gupta VK (2015) Removal of basic dye Auramine-O by ZnS: cu nanoparticles loaded on activated carbon: optimization of parameters using response surface methodology with central composite design. RSC Adv 5: 18438–18450
61. Gupta VK, Atar N, Yola ML, Üstündağ Z, Uzun L (2014) A novel magnetic Fe@au core–shell nanoparticles anchored graphene oxide recyclable nanocatalyst for the reduction of nitrophenol compounds. Water Res 48(1):210–217
62. Gupta VK, Jain CK, Ali I, Chandra S, Agarwal S (2002) Removal of lindane and malathion from wastewater using bagasse fly ash—a sugar industry waste. Water Res 36(10):2483–2490
63. Saravanan R, Gupta VK, Narayanan V, Stephen A (2013) Comparative study on photocatalytic activity of ZnO prepared by different methods. J Mol Liq 181:133–141
64. Nodeh HE, Ibrahim WAW, Ali I, Sanagi MM (2016) Development of magnetic graphene oxide adsorbent for the removal and preconcentration of as(III) and as(V) species from environmental water samples. Environ Sci Pollut Res 23:9759–9773
65. Ali I, Gupta VK, Khan TA, Asim M (2012) Removal of arsenate from aqueous solution by electrocoagulation method using Al-Fe electrodes. Int J Electrochem Sci 7(2012):1898–1907
66. Devaraj M, Saravanan R, Deivasigamani RK, Gupta VK, Gracia F, Jayadevan S (2016) Fabrication of novel shape Cu and Cu/Cu2O nanoparticles modified electrode for the determination of dopamine and paracetamol. J Mol Liq 221:930–941
67. Girgis BS, El-Hendawy AA (2002) Porosity development in activated carbons obtained from date pits under chemical activation with phosphoric acid. Microporous Mesoporous Mater 52:105–117
68. Venersson T, Bonelli PR, Cerella EG, Cukierman AL (2002) *Arundo donax* cane as a precursor for activated carbons preparation by phosphoric acid activation. Bioresour Technol 83:95–104

69. Guo J, Lua AC (2003) Adsorption of Sulphur dioxide unto activated carbon prepared from oil-palm shells with and without pre-impregnation. Sep Purif Technol 30:265–273
70. Diao Y, Walawender WP, Fan LT (2002) Activated carbons prepared from phosphoric acid activation of grain sorghum. Bioresour Technol 8(1):45–52
71. Benaddi H, Legras D, Rouzaud JN, Beguin F (1998) Influence of the atmosphere in the chemical activation of wood by phosphoric acid. Carbon 36:306–309
72. Fierro V, Torne-Fernandez V, Montane D, Celzard A (2005) Study of the decomposition of Kraft lignin impregnated with orthophosphoric acid. Thermochim Acta 433:142–148
73. Bello OS, MohdAzmier A, Northidayah A (2012) Adsorptive features of banana (*Musa paradisiaca*) stalk -based activated carbon for malachite green dye removal. Chem Ecol 28(2):153–167
74. Ogunleye OO, Adio O, Salawudeen TO (2014) Removal of lead (II) from aqueous solution using banana (*Musa paradisiaca*) stalk-based activated carbon. Chemical and Process Engineering Research 28:45–59
75. Olakunle MO, Inyinbor AA, Dada AO, Bello OS (2017) Combating dye pollution using cocoa pod husks: a sustainable approach. Int J Sustain Eng 11(1):4–15
76. Qu Y (2009) Equilibrium and kinetics study on the adsorption of perfluorooctanoic acid from aqueous solution onto powdered activated carbon. J Hazard Mater 169(1–3):146–152
77. Ahmad MA, Alrozi R (2011) Removal of malachite green dye from aqueous solution using rambutan peel-based activated carbon: equilibrium, kinetic and thermodynamic studies. Chem Eng J 171(2):510–516
78. Ahmad MA, Ahmad N, Bello OS (2014) Adsorption kinetic studies for the removal of synthetic dye using durian seed activated carbon. J Dispers Sci Technol 36(5):670–684
79. Boehm HP (1966) Chemical identification of surface groups. Adv Catal 16(179–274):360–564
80. Russel WB, Saville DA, Schowalter WR (1989) Colloidal dispersions, vol 525.*University Press, Cambridge*, pp. 250
81. Bello OS, Owojuyigbe ES, Babatunde MA, Folaranmi FE (2017) Sustainable conversion of agro-wastes into useful adsorbents. Appl Water Sci 7:3561–3571
82. Kooh MRR, Dahri MK, Lim LBL (2016) The removal of Rhodamine B dye from aqueous solution using *Casuarina equisetifolia* needles as adsorbent. Cogent Environmental Science 2:1–14
83. Ojedokun AT, Bello OS (2017) Kinetic modeling of liquid-phase adsorption of Congo red dye using guava leaf-based activated carbon. Appl Water Sci 7:1965–1977
84. Bello OS, Ahmad MA (2012) Coconut (*Cocos nucifera*) shell-based activated carbon for the removal of malachite green dye from aqueous solutions. Sep Sci Technol 47:903–912
85. Bhadusha N, Ananthabaskaran T (2011) Adsorptive removal of methylene blue onto $ZnCl_2$ activated carbon from wood apple outer shell: kinetics and equilibrium studies. E-Journal of Chemistry 8:1696–1707
86. Baek MH, Ijagbemi CO, SJ O, Kim DS (2010) Removal of malachite green from aqueous solution. J Hazard Mater 176:820–828
87. Singh M, Dosanjh HS, Singh H (2016) Surface modified spinel cobalt ferrite nanoparticles for cationic dye removal: kinetics and thermodynamics studies. Journal of Water Process Engineering 11:152–161
88. Dube C, Tandlich R, Wilhelmi B (2018) Adsorptive removal of ciprofloxacin and isoniazid from aqueous solution. Nova Biotechnologica et Chimica 17(1):16–28
89. Hossain MA, Ngo HH, Guo WS, Nguyen TV (2012) Biosorption of cu (II) from water by banana peel based biosorbent: experiments and models of adsorption and desorption. Journal of Water Sustainability 2(1):87–104
90. Wu HX, Wang TJ, Chen L, Jin Y (2009) The roles of the surface charge and hydroxyl group on a Fe-Al-Ce adsorbent in fluoride adsorption. Ind Eng Chem Res 48:4530–4534
91. MohdYasim NSE, Ismail ZS, Zaki SM, Azis MFA (2016) Adsorption of cu, as, Pb and Zn by banana trunk. Malaysian Journal of Analytical Sciences 20(1):187–196
92. Farahani M, Abdullah SRS, Hosseini S et al (2011) Adsorption-based cationic dyes using the carbon active sugarcane bagasse. Procedia Environ Sci 10(Part A):203–208
93. Li S, Zhang X, Huang Y (2017) Zeolitic imidazolate framework-8 derived nano porous carbon as an effective and recyclable adsorbent for removal of ciprofloxacin antibiotics from water. J Hazard Mater 321:711–719
94. Cheng R, Li H, Liu Z, Du C (2018) Halloysite nanotubes as an effective and recyclable adsorbent for removal of low concentration antibiotics ciprofloxacin. Minerals 8:378–387
95. Aborode AT (2020) Adsorption of ciprofloxacin HCl from aqueous solution using activated kaolin. World Scientific News 145: 62–73
96. Budinova T, Ekinci E, Yardim F, Grimm A, Björnbom E, Minkova V, Goranova M (2006) Characterization and application of activated carbon produced by H_3PO_4 and water vapor activation. Fuel Process Technol 87:899–905
97. Li J, Yu G, Pan L, Li C, You F, Xie S, Wang Y, Ma J, Shang X (2018) Study of ciprofloxacin removal by biochar obtained from used tea leaves. J Environ Sci 73:20–30. https://doi.org/10.1016/j.jes.2017.12.024
98. Kumar KV, Kumaran A (2005) Removal of methylene blue by mango seed kernel powder. Biochem Eng J 27(1):83–93
99. Li Y, Du Q, Liu T, Sun J, Jiao Y, Xia Y et al (2012) Equilibrium, kinetic and thermodynamic studies on the adsorption of phenol onto graphene. Mater Res Bull 47(8):1898–1904
100. Zeng Z, Tan X, Liu Y, Tian S, Zeng G, Jiang L, Liu S, Li J, Liu N, Yin Z (2018) Comprehensive adsorption studies of doxycycline and ciprofloxacin antibiotics by biochars prepared at different temperatures. Frontiers in Chemistry 6:80–81
101. Ali I, Burakova I, Galunin E, Burakov A, Mkrtchyan E, Melezhik A, Kurnosov D, Tkachev A, Grachev V (2019) High-speed and high-capacity removal of methyl orange and malachite green in water using newly developed mesoporous carbon: kinetic and isotherm studies. ACS Omega 4:19293–19306
102. Dehghani MH, Alimohammadi M, Mahvi AH, Rastkari N, Mostofi M, Gholami M (2014) Performance of multiwall carbon nanotubes for removal phenol from aqueous solutions. Iran Journal of Health Environment 6(4):491–502
103. Sharifpour N, Moghaddam FM, Mardani G, Malakootian M (2020) Evaluation of the activated carbon coated with multiwalled carbon nanotubes in removal of ciprofloxacin from aqueous solutions. Appl Water Sci 10:140
104. Nekouei F, Nekouei S, Tayagi IJ, Gupta VK (2014) Kinetic, thermodynamic and isotherm studies for acid blue 129 removal from liquids using copper oxide nanoparticle-modified activated carbon as a novel adsorbent. J Mol Liq 198:409–412
105. Helfferich F (1962) Ion-exchange, McGraw-Hill New York, 335–360
106. Ali I, Alexandr EB, Alexandr VM, Alexandr VB, Irina VB, Elena AN, Evgeny VG, Alexey GT, Denis VK (2019) Removal of copper (II) and zinc (II) ions in water on a newly synthesized polyhydroquinone/graphene nanocomposite material: kinetics, thermodynamics and mechanism. Chemistry Select 4:12708–12718
107. Gu C, Karthileyan G (2005) Sorption of the antimicrobial ciprofloxacin to aluminum and iron hydrous oxides. Environ Sci Technol 39:9166–9173

108. Li Z, Hong H, Liao L, Ackley CJ, Schulz LA, MacDonald RA, Emard SMA (2011) Mechanistic study of ciprofloxacin removal by kaolinite. Colloids Surf B: Biointerfaces 88:339–344
109. Mutasim E, Elhussien MAA, Rashida MH, Mawia HE (2017) Removal of ciprofloxacin hydrochloride from aqueous solution by pomegranate peel grown in Alziedab agricultural scheme - River Nile state, Sudan. Advances in Biochemistry 5(5):89–96
110. Nahid K, Shahin A, Ferdos KM (2017) Kinetic and isotherm studies on ciprofloxacin an adsorption using magnesium oxide nanoparticles. J Appl Pharm Sci 7(11):079–083
111. Davoud B, Ferdos KM, Ali J (2017) Kinetics and mechanism of red mud in adsorption of ciprofloxacin in aqueous solution. Biosci Biotechnol Res Commun 10(1):241–248
112. Li R, Wang Z, Guo J, Li Y, Zhang H, Zhu J, Xie X (2018) Enhanced adsorption of ciprofloxacin by KOH modified biochar derived from potato stems and leaves. Water Sci Technol 77(4): 1127–1136
113. Lin C-C, Lee C-Y (2020) Adsorption of ciprofloxacin in water using Fe_3O_4 nanoparticles formed at low temperature and high reactant concentrations in a rotating packed bed with co-precipitation. Mater Chem Phys 240:122049
114. Duan W, Wang N, Xiao W, Zhao Y, Zheng Y (2018) Ciprofloxacin adsorption onto different micro-structured tourmaline, halloysite and biotite. J Mol Liq 269:874–881
115. Zhao J, Liang G, Zhang X, Cai X, Li R, Xie X, Wang Z (2019) Coating magnetic biocharwith humic acid for high efficient removal of fluoroquinolone antibiotics in water. Sci Total Environ 688:1205–1215
116. Wang L, Chen G, Ling C, Zhang J, Szerlag K. (2017) Adsorption of ciprofloxacin on to bamboo charcoal: effects of pH, salinity, cations, and phosphate Environmental Progress & Sustainable Energy DOI https://doi.org/10.1002/ep.12579
117. Wang L, Yang C, Lu A, Liu S, Pei Y, Luo X (2020) An easy and unique design strategy for insoluble humic acid/cellulose nanocomposite beads with highly enhanced adsorption performance of low concentration ciprofloxacin in water. Bioresour Technol 302:122812
118. Wu S, Zhao X, Li Y, Zhao C, Du Q, Sun J, Wang Y, Peng X, Xia Y, Wang Z, Xia L (2013) Adsorption of ciprofloxacin onto biocomposite fibers of graphene oxide/calcium alginate. Chem Eng J 230:389–395
119. Tam NT, Liu Y, Bashir H, Yin Z, He Y, Zhou X (2020) Efficient removal of diclofenac from aqueous solution by potassium ferrate-activated porous graphitic biochar: ambient condition influences and adsorption mechanism. Int J Environ Res Public Health 17: 291
120. Wang CJ, Li ZH, Jiang WT, Jean JS, Chuan CC (2010) Cation exchange interaction between antibiotic ciprofloxacin and montmorillonite. J Hazard Mater B 183(1–3):309–314
121. Punyapalakul P, Sitthisorn T (2010) Removal of ciprofloxacin and carbamazepine by adsorption on functionalized mesoporous silicates. World Acad Sci Eng Technol 69:546–550
122. El-Shafey EI, Al-Lawati H, Al-Sumri AS (2012) Ciprofloxacin adsorption from aqueous solution onto chemically prepared carbon from date palm leaflets. J Environ Sci 24(9):1579–1586
123. Staudt J, Scheufele FB, Ribeiro C, Sato TY, Canevesi R, Borba CE (2020) Ciprofloxacin desorption from gel type ion exchange resin: desorption modeling in batch system and fixed bed column. Sep Purif Technol 230:115857
124. Momina MS, Isamil S (2020) Study of the adsorption/desorption of MB dye solution using bentonite adsorbent coating. Journal of Water Process Engineering 34:101155